Available online at www.sciencedirect.com
ScienceDirect
Journal of the European Ceramic Society 28 (2008) 1899–1907
www.elsevier.com/locate/jeurceramsoc

Arc-jet testing on HfB_2 and HfC-based ultra-high temperature ceramic materials

Raffaele Savino [a,*], Mario De Stefano Fumo [a], Laura Silvestroni [b], Diletta Sciti [b]

[a] *Dipartimento di Ingegneria Aerospaziale, University of Naples "Federico II", P.le V. Tecchio 80, 80125 Naples, Italy*
[b] *ISTEC, Institute of Science and Technology for Ceramics, CNR, Via Granarolo 64, 48018 Faenza, Italy*

Received 25 July 2007; received in revised form 13 November 2007; accepted 25 November 2007
Available online 4 March 2008

Abstract

The behaviour of pressureless sintered HfC and HfB_2 ceramics, when exposed to high enthalpy plasma flows typical of atmospheric re-entry environment, was investigated with an arc-jet facility at temperatures exceeding 2000 °C. The surface temperature and emissivity of the materials were evaluated during the test. The microstructure modifications were analysed after exposure. Fluid dynamic numerical simulations were carried out to evaluate the catalytic atom recombination efficiencies of the materials at the experimental conditions. Surface and cross sections of the samples showed the formation of scales mainly consisting of HfO_2 and SiO_2. For the HfB_2-based composite numerical results correlated quite well with experimental ones assuming a low catalytic surface behaviour. For the HfC-based material the surface behaviour changed from low catalytic to partially catalytic as the temperature increased. The post-test analyses confirm the potential of these composites to endure re-entry conditions with temperature approaching 2000 °C or even higher.

Keywords: Arc-jet; Thermal protection systems; HfB_2; HfC; Oxidation

1. Introduction

Ultra-high temperature ceramics (UHTCs) are currently considered as emerging materials for aerospace applications.[1–4] The increasing attention is driven by the demand of developing reusable hot structures as thermal protection systems (TPS) of re-entry vehicles characterised by sharp leading edges and therefore by larger aerothermal heating than blunt edges, such as those on the Space Shuttle, able to withstand temperatures that may exceed 2000 °C during re-entry. As available materials cannot survive such extreme temperatures, new ones are required for advanced thermal protection systems.[1,4,5] The use of UHTCs for sharp leading edges would also imply lower aerodynamic drag, improved flight performances and crew safety, due to the larger cross range and manoeuvrability along with more gentle re-entry trajectories.[3,6,7]

Hafnium boride and hafnium carbide, belonging to the class of the UHTCs, are candidates for thermal protection materials in both re-entry and hypersonic vehicles because of their high melting points (~3900 °C) and excellent chemical stability.[8–13] Other notable properties are their high hardness, high electrical and thermal conductivity.[8–13] Despite all the potentialities, so far these compounds have not been developed on industrial scale due to the difficult sinterability and low fracture toughness. Recent studies have pointed out that the addition of $MoSi_2$ as sintering aid allows the achievement of highly dense bodies (98%) at 1950 °C by pressureless sintering.[14,15] Furthermore, the addition of $MoSi_2$ is expected to improve the oxidation resistance due to the development of a silica protective coating.[16]

In this paper, arc-jet testing at temperatures between 1950 °C and 2400 °C is carried out on pressureless sintered HfB_2 and HfC-based materials. Arc-jet testing represents the best ground-based simulation of a re-entry environment, in different ways. On one hand, it provides the possibility to explore the oxidation behaviour of these materials under extreme conditions. On the other hand, the materials response to large heat fluxes is evaluated through the determination of two important parameters, i.e. emissivity and catalytic efficiency. High values of emissivity and low values of surface catalytic efficiency are desired for

* Corresponding author. Tel.: +39 0817682357; fax: +39 0815932044.
E-mail address: rasavino@unina.it (R. Savino).

0955-2219/$ – see front matter © 2008 Elsevier Ltd. All rights reserved.
doi:10.1016/j.jeurceramsoc.2007.11.021

Table 1
Starting materials: compositions, densities, thermal properties and emissivity

Label	Composition (vol%)	Sintering cycle	Bulk density (g/cm^3)	Relative density (%)	Mean grain size (μm)	Emissivity
HB5	HfB_2 + 5% $MoSi_2$	1950 °C/60 min	10.7	98	1.5	0.9 (1600–2000 °C)
HC5	HfC + 5% $MoSi_2$	1950 °C/60 min	12.1	98	3.0	0.7 (1800–2400 °C)

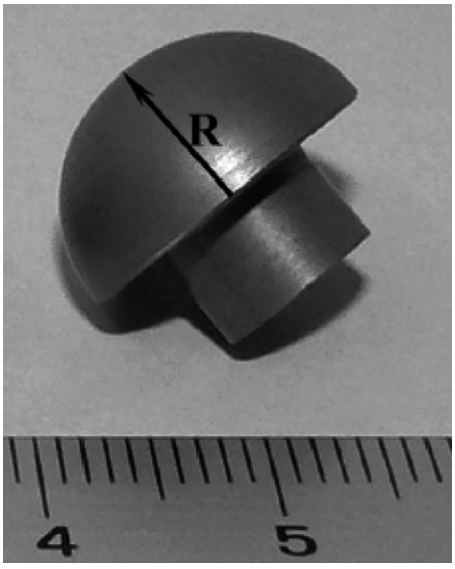

Fig. 1. Hemispheric HfB_2 model used for arc-jet testing, curvature radius $R = 7.5$ mm.

the above mentioned applications as they reduce temperature gradients and thermal stresses in the structure, thus enabling the vehicle to operate under relatively high enthalpy flow conditions. So far, ZrB_2–SiC and HfB_2–SiC composites were the predecessor materials analysed by arc-jet testing in the literature of UHTCs.[3,17]

Microstructural modifications induced by high thermal loading are investigated and discussed. In addition, fluid dynamic numerical simulations are carried out in order to rebuild, through computational fluid dynamic (CFD) modelling, the experimental tests and to evaluate an average catalytic efficiency of the different materials with respect to oxygen and nitrogen surface recombination reactions.

2. Experimental

2.1. Material processing and characterisation

The following materials were selected for the arc-jet tests:

HfB_2 + 5 vol% $MoSi_2$, labelled as HB5.
HfC + 5 vol% $MoSi_2$, labelled as HC5.

Commercial powders were used to prepare the ceramic materials: HfB_2 (Cerac Incorporated, Milwaukee, USA), particle size range 0.5–5 μm, impurities: Al (0.07%), Fe (0.01%), Zr (0.47%); Cubic HfC (Cerac Inc., USA), 325 mesh, fisher size 1.1 μm, grain size range 0.2–1.5 μm; Tetragonal $MoSi_2$ (<2 μm, Aldrich, USA), mean particle size 2.8 μm, grain size range 0.3–5 μm and oxygen content ∼1 wt%.

The powder mixtures were ultrasonically treated and milled for 24 h in absolute ethanol using zirconia milling media, then dried in a rotary evaporator and sieved to −250 mesh screen size. Four-centimetre diameter pellets were linearly pressed and subsequently cold isostatically pressed under 350 MPa before sintering. The pellets were pressureless sintered in a resistance-heated graphite furnace under a flowing argon atmosphere (∼1 atm) at 1950 °C for 60 min. The bulk density was measured with the Archimedes method. The relative density was calculated dividing the bulk density by the theoretical density that was evaluated with the rule of mixture on the basis of the starting compositions. The dense samples were examined using X-ray diffraction (Siemens D500, Germany) to identify crystalline phases. The microstructures were polished with diamond paste to 0.25 μm and were analysed with scanning electron microscopy (SEM, Cambridge S360) and energy dispersive spectroscopy (EDS, INCA Energy 300, Oxford instruments, UK). The main properties of the processed materials are summarized in Table 1. After the arc-jet tests, the ceramic models

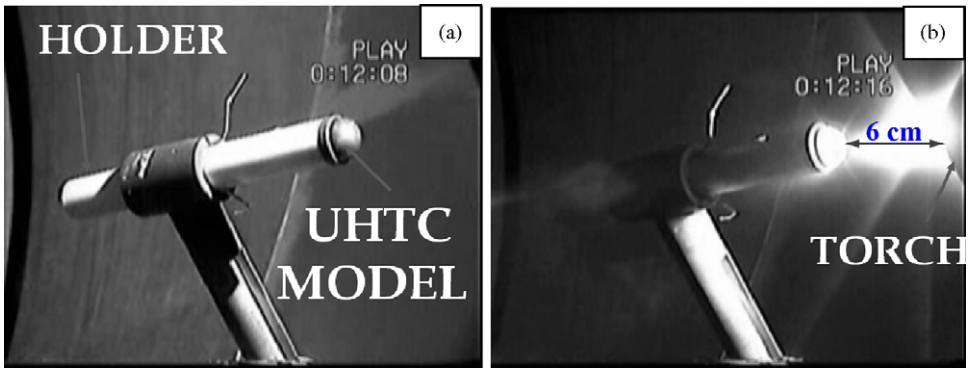

Fig. 2. Experimental setup. (a) Before the test and (b) during the test.

were further analysed by SEM–EDS on surface and cross section.

2.2. Plasma torch tests

Samples with a hemispheric shape (Fig. 1) were machined through diamond-loaded tools and then exposed to sustained enthalpy flows using the arc-jet facility equipped with a 80 kW plasma torch that operates in inert gas (He, N_2, Ar and their mixtures) at mass flow rates up to 5 g/s. The specimens were located at a distance of 6 cm from the exit torch. (Fig. 2a and b) The HfB_2-based model was tested with an initial average specific total enthalpy of about 20 MJ/kg, that was gradually increased tuning the arc current up to 26 MJ/kg and then maintained for approximately 30 s. HfC-based models were exposed to hot streams at two different conditions. The first test denoted as HC5-I, was conducted setting the initial average specific total enthalpy at 20 MJ/kg for about 40 s; then a value of 22 MJ/kg was achieved and maintained for about 60 s. During the second test, denoted as HC5-II, the specific total enthalpy was set at 22 MJ/kg during the first 90 s, 24 MJ/kg during the following 60 s and 26 MJ/kg during the last 240 s.

During the experiments, infrared and optical windows in the test chamber allowed visual inspection and diagnostic analyses. An automatic control system monitored the main parameters of the apparatus (voltage and current of the arc heater, water cooling temperature and mass flow rate). In particular, the specific total enthalpy (H) was evaluated through an energy balance between the energy supplied to the gas by the arc heater and the energy transferred to the cooling system (measured by the water temperature jump between inlet and outlet). The output data, processed via a dedicated software, allowed the evaluation of the surface temperature profile versus exposure time of the mode. Due to the extremely high thermal loading upon the ceramic models, surface chemical reactions like oxidation can be responsible for changes in the material's emissivity. To overcome this problem, the experiments' measurements were carried out with a radiation ratio pyrometer (Infratherm ISQ5, Impac Electronic Gmbh, Germany) which operates both in two colour and in the single colour function. In the two colour mode the instrument makes use of the ratio of two spectral radiances, measured at different wavelengths (0.9–1.05 μm), to evaluate the true temperature. This overcomes the problem of the emissivity knowledge since it is supposed to be the same at both wavelengths. Once the temperature was measured with the ratio pyrometer, its value was input to evaluate the spectral emissivity using the single colour function ($\lambda = 0.9$ μm). In combination with the pyrometer, an infrared thermo-camera (Thermacam SC 3000, FLIR Systems, USA) was used to measure the surface temperature distributions and the spectral emissivity in the long wave range of the thermograph ($\lambda = 9$ μm).

2.3. Numerical simulation of the plasma torch flow

To assess if the environment generated by the plasma torch at atmospheric pressure was able to reproduce heat fluxes, temperatures and reactive environments typical of atmospheric re-entry conditions, a systematic numerical analysis was carried out. The computations were carried out solving the full Navier–Stokes equations for a turbulent multi-reacting gas mixture with six chemical species (Ar, O, O_2, NO, N and N_2) in chemical non-equilibrium. Each species of the mixture was assumed to behave as a thermally perfect gas, where translational–rotational and vibrational–electronic degrees of freedom were characterised by different temperatures. Vibrational–translational energy exchanges were modelled according to the Landau–Teller model, while the vibrational relaxation time was derived from the Millikan–White formula, with Park correction for high temperatures.[18] Chemical and vibrational non-equilibrium was taken into account using the Park model.[19–21] The fluid dynamics equations were numerically solved in the computational domain (plasma torch and test chamber). Convective fluxes were computed according to Roe's Flux Difference Splitting scheme. Integration of the equations was implicit in time performed, until steady state was achieved, solving the linearised system of equation by the multigrid technique.

3. Results and discussion

3.1. Microstructural features of the as-sintered samples

3.1.1. HfB_2-based composite

According to X-ray diffraction analysis (not shown), the sintered specimen was constituted by hexagonal HfB_2 and

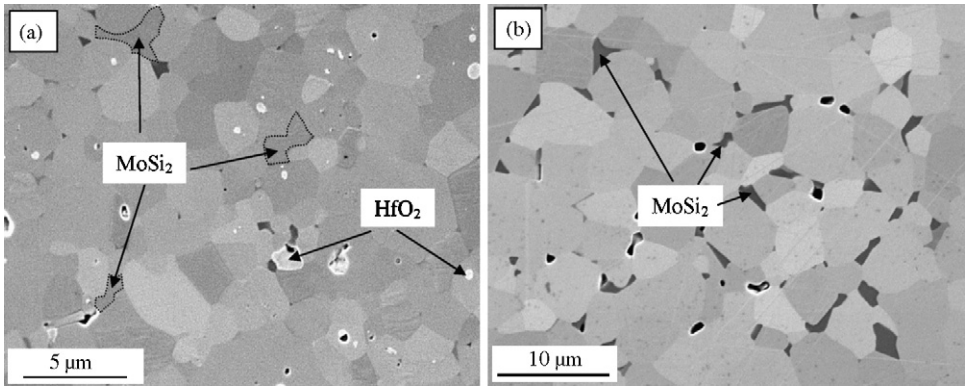

Fig. 3. Polished surfaces of (a) HfB_2- and (b) HfC-based composites.

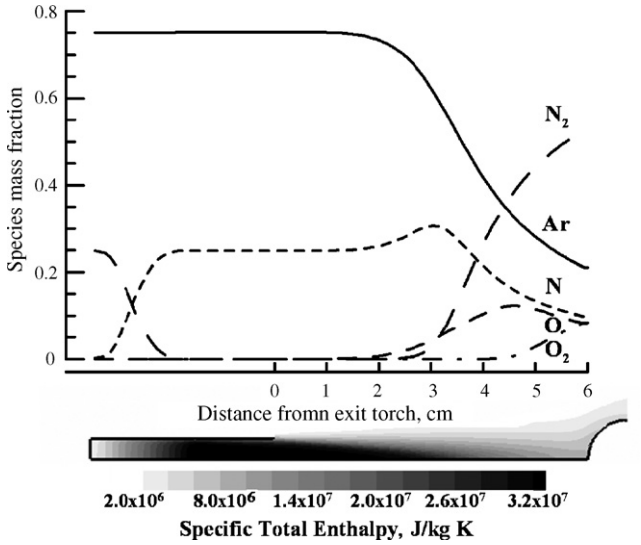

Fig. 4. Computed mass fractions of the different species along the torch axis and specific total enthalpy contour. $H = 26$ MJ/kg.

tetragonal $MoSi_2$ and monoclinic HfO_2.[14] The relative density was 98%, as reported in Table 1. The polished section (Fig. 3a) showed a regular microstructure, with little residual porosity. HfB_2 grains had a rounded shape with mean grain size estimated by image analysis of about 1.5 μm, while the $MoSi_2$ phase had an irregular morphology with very low dihedral angles (20–30°). This peculiar characteristic indicates that $MoSi_2$ was very ductile at the sintering temperature and was accommodated between the voids left by the HfB_2 skeleton. Further details are reported elsewhere.[14]

3.1.2. HfC-based composite

Cubic HfC and tetragonal $MoSi_2$ were the crystalline phases detected after sintering. The final density was 98% (Table 1). The typical microstructure of the HfC-based composite is shown in Fig. 3b. Very few porosity was detected by SEM inspections on this material. HfC grains had a squared shape and displayed a bright colour, while the $MoSi_2$ phase had an irregular shape and was recognizable as a darker contrast phase. The mean grain size of the carbide grains was about 3 μm (Table 1). Further details are reported in an earlier work.[15]

3.2. Plasma flow characterisation

The results herein presented refer to a 75% argon–25% nitrogen mixture plasma jet with mass flow rate of 1.45 g/s, for an average specific total enthalpy of the flow at the torch exit varying from 20 MJ/kg to 28 MJ/kg, at atmospheric pressure. At the exit of the torch the plasma containing argon, nitrogen and atomic nitrogen expands through a nozzle (5 mm in diameter), comes into contact with the surrounding air at ambient conditions, so that oxygen in the atmosphere dissociates and a reacting mixture composed of Ar, O_2, N_2, NO, O and N is formed. Fig. 4 shows the results of computations performed for the case of an average specific total enthalpy of 26 MJ/kg. According to the calculations, the average specific total enthalpy in proximity of the specimen reduces drastically to about 6–8 MJ/kg (Fig. 4). Table 2 summarizes the test conditions and the computed flow characteristics for the different experiments. Correspondingly, Fig. 5a and b shows the increase of the surface temperature as a function of the exposition time for HfB_2 and HfC samples, respectively. It must be mentioned that the temperature reached at the sample surface depends on the ability of the material to reject the heat by radiation, i.e. on its emissivity ($\varepsilon = 1$ for an ideal black body, $\varepsilon < 1$ for a real material surface). The higher is the emissivity, the greater is the emitted radiation. However, the temperature of the sample also depends on its thermal conductivity, since a high thermal conductivity allows heat to be conducted from the leading edge to colder zones and from there to be radiated away. The maximum temperature reached on the surface of HfB_2 sample was 1950 °C, Fig. 5a. The corresponding stagnation point heat flux, computed by numerical simulation was in the range 5–8 MW/m^2. A value of about 0.9 was estimated

Table 2
Test conditions

Flow conditions	Arc power (kW)			
	38.0	42.5	46.0	51.0
Exit torch conditions				
Average specific total enthalpy (MJ/kg)	20	22	24	26
Temperature (°C)	17,500	19,300	21,000	23,000
Flow conditions at model location				
Specific total enthalpy (MJ/kg)	5.8	6.5	7.1	8.0
Temperature (°C)	2900	3200	3400	3800
Ar mass fraction	0.21	0.21	0.21	0.21
N_2 mass fraction	0.55	0.55	0.53	0.52
N mass fraction	0.076	0.08	0.09	0.10
O_2 mass fraction	0.12	0.11	0.1	0.08
O mass fraction	0.046	0.05	0.07	0.08
NO mass fraction	0	0	0	0
Stagnation point				
Pressure (Pa)	114,000	116,000	119,000	122,000
Non catalytic heat flux (MW/m^2)	5	6	7	8

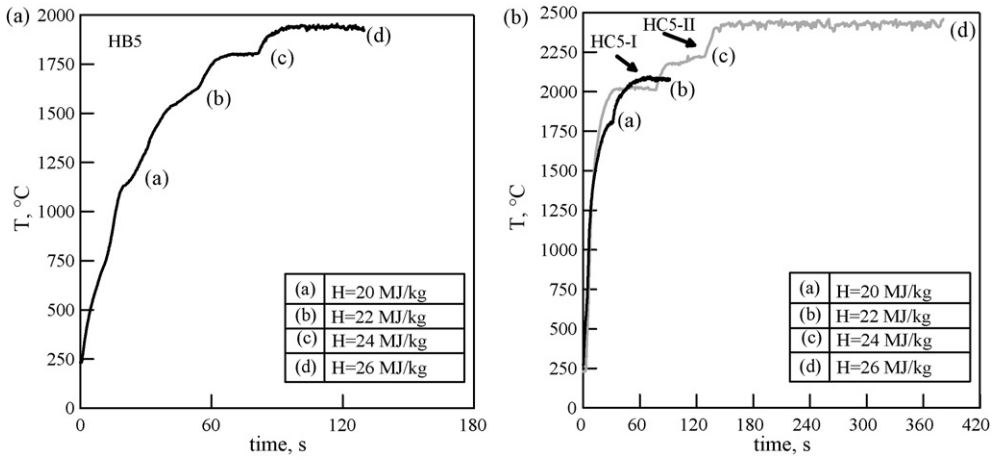

Fig. 5. Temperature profiles vs. time during arc-jet testing of the (a) HB5 and (b) HC5-I and HC5-II models corresponding to specific total enthalpies during the test.

for the emissivity at the highest temperature. During the first test on HfC model (HC5-I), the surface temperature achieved by the sample was 2050 °C (Fig. 5b). During the second test (HC5-II) the surface temperature reached the value of 2400 °C that was maintained for about 4 min. The corresponding computed surface heat flux was of the order of 10 MW/m^2. In both tests a value of about 0.7 was measured for the emissivity at the highest temperatures. The emissivity values of the samples, tested at different conditions, were found to be independent of the test temperature and conditions. These values were similar to those found for other ZrB_2–SiC ultra-high temperature ceramics tested in similar conditions.[17,22]

Both the boride and carbide materials showed an excellent stability during the tests, despite the unavoidable microstructural changes occurring on their surface, as described below.

3.3. Microstructural modifications induced by high enthalpy plasma

3.3.1. HfB_2 sample

Due to high thermal loading and the presence of oxidising species, oxidation of the constituent phases occurred. The sample surface was covered by a compact silica-based scale (15–20 μm thick), which embedded HfO_2 crystals (Fig. 6a). The composition of the outer glassy layer was investigated by means of EDS analysis. The silica-based scale contained several impurities, including Hf, Al and boron. Bubble formation is due to evolution of gaseous products. The shear forces associated to the hot stream enhanced the bursting of bubbles. The analysis of the cross section (Fig. 6c) revealed that the scale was a multilayered oxide (~70 μm thick) well adherent to the bulk, implying that no micro/macrospallation phenomena occurred. Underneath the surface silica oxide (about 10 μm), the scale was mainly constituted by large HfO_2 grains and silica with composition close to SiO_2 (Fig. 6e). Occasionally Al impurities were detected inside the glassy phase. In the innermost layer formation of molybdenum oxides, silicon oxides and hafnium oxide was observed. Nitrogen impurities were also detected in the composition of the molybdenum-based oxide. The chemistry of the experiment carried out on HfB_2-based material was governed by the oxidation reaction of the two constituent phases. Hafnium diboride oxidises according to[23]:

$$HfB_2(s) + (5/2)O_2(g) = HfO_2(s) + B_2O_3(l) \quad (1)$$

$$B_2O_3(l) = B_2O_3(g) \quad (2)$$

Hafnia is a very stable phase in oxidising atmosphere above 2000 °C. It has a melting point of 2900 °C and relatively low vapour pressure.[24] Boron oxide has a low melting point and high vapour pressure, therefore at $T > 1100$ °C, it starts to evaporate, according to reaction (2). On the other hand, at temperatures > 1000 °C, $MoSi_2$ is known to form a stable silica layer according to[25]:

$$MoSi_2 + (7/2)O_2(g) = MoO_3(g) + 2SiO_2 \quad (3)$$

The nature of the oxide observed suggests that during the plasma torch tests the silica production according to reaction (3) was fast enough to protect the material. The formation of bubble was produced by the escape of gaseous by-products, such as MoO_3, B_2O_3 and other highly volatile boron suboxides. However, the presence of B impurities in the outer glassy layer suggests that due to the short exposure the release of boron gaseous products was not complete. The role of dissociated oxygen, which is the primary oxidant agent in a re-entry environment, is still matter of debate. Substituting atomic oxygen to molecular oxygen, thermodynamic calculations (HSC Chemistry for Windows 5, Outokompu Research, OY, Pori, Finland) indicate that reactions (2) and (3) are even more favoured (the absolute value of free Gibbs energy increases by a factor comprised between 1.4 and 1.7). Preliminary results reported in the literature on ZrB_2–SiC composites subjected to re-entry simulations confirmed that oxidation by atomic oxygen proceeds more rapidly than by molecular oxygen.[4]

Post-tests analyses unfortunately do not help to clarify these aspects. The morphology of the cross section, despite the drastic differences in the experimental conditions, is very similar to that of HfB_2–$MoSi_2$ composites oxidised under conventional conditions, such as static air, longer holding times (15 min) and temperatures of 1400–1650 °C. Recent studies[11] confirm that the response of ZrB_2–SiC and HfB_2–SiC ceramics to arc heater

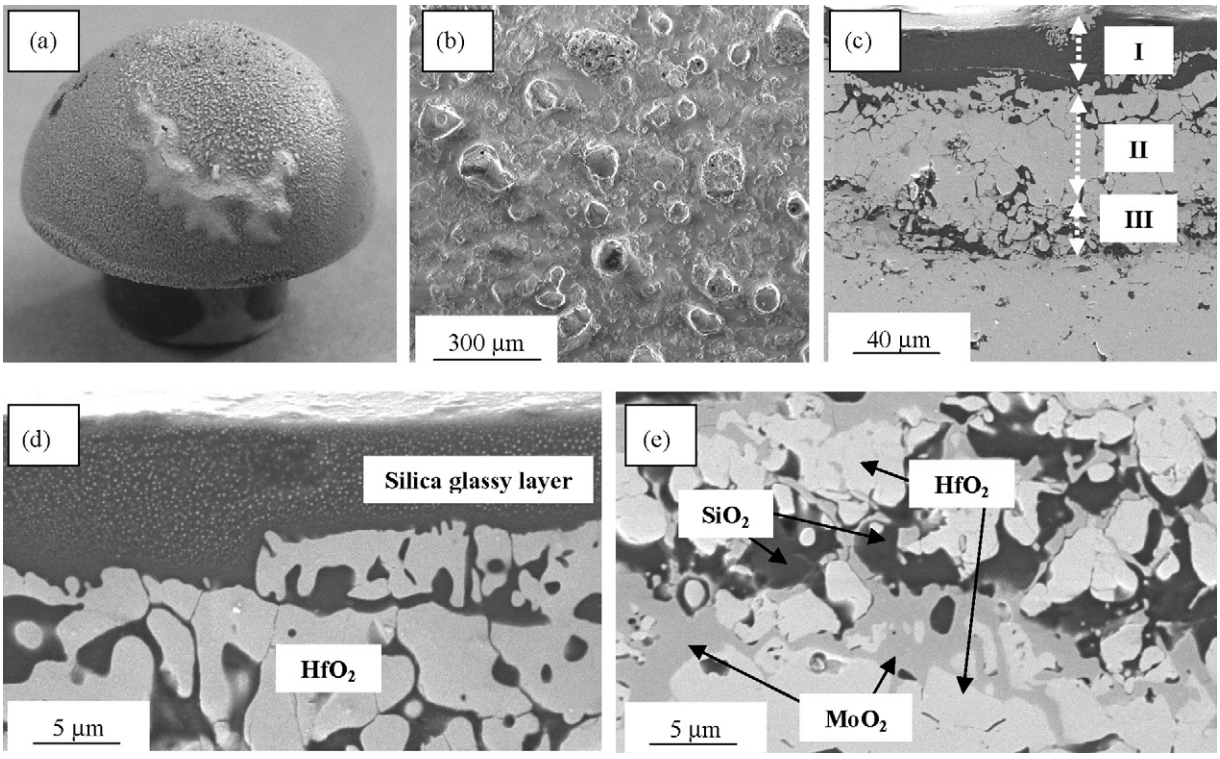

Fig. 6. (a) HfB_2 sample after arc-jet test, (b) surface, (c) cross section, (d) enlarged view of layers I, II and (e) Enlarged view of layer III.

testing appear to be similar to conventional oxidation studies. Finally, it is worth noting that differently from ZrB_2–SiC and HfB_2–SiC composites no depletion layer was observed in the scale, i.e. no active oxidation of $MoSi_2$ occurred for this system.

3.3.2. *HfC samples*

After the HFC-I tests no significant variation of the sample size and shape was observed, implying that the extent of ablation was very low. The surface turned from dark grey to a whitish colour (Fig. 7a and b) and was constituted by a visibly cracked hafnium oxide scale, with no glassy phase. The specimen section (Fig. 7c) displayed the formation of a multilayered scale, with thickness of about 90 μm, well adherent to the unreacted bulk. Underneath the surface, the outermost portion of the scale was constituted by hafnium oxide and a silica-based glassy phase, which partially filled the porosity (Fig. 7d). The intermediate layer contained a fine porosity and was constituted by hafnia and isolated pockets of molybdenum oxide (Fig. 7e). The innermost layer contained partially oxidised HfC and SiC, and residual Mo–Si species (Fig. 7f). No porosity was found in this region. Similar features were displayed by the model tested at 2400 °C (test HfC-II), even if the oxide scale (∼300 μm thick) was found to be partially detached from the unreacted bulk.

Despite the presence of $MoSi_2$ as a SiO_2-forming phase, no evidence of continuous glassy layer was found on the surface of HfC, in contrast with results obtained for HfB_2. This finding cannot be totally imputed to the extreme conditions of the present experiments. The two compositions, HB5 and HC5, were in fact oxidised at the same conditions, in static air (i.e. in absence of significant ablation) at 1650 °C, in a conventional furnace. Even under these milder conditions, HfB_2 displayed the formation of a compact layer of silica, while the surface of HfC was mainly covered by an HfO_2 scale with few discontinuous pockets of silica. This experiment suggests that the presence of a carbide matrix rather than a boride apparently hindered the formation of a stable silica layer. It can be hypothesized that CO species deriving from oxidation of HfC interacted with $MoSi_2$ causing release of volatile SiO.

In the cross section, the layered structure of the oxide (Fig. 7) resemble the results presented in the literature on the oxidation behaviour of monolithic HfC[24,26] These studies reported the formation of a layered scale, which comprised a porous outer layer, a dense interlayer and an oxycarbide layer, $HfO_{2-x}C_y$.[24,26] The addition of $MoSi_2$ in the composite of the present work resulted in formation of silica which partially filled the inner porosity of the HfO_2 scale, a feature which should improve its oxidation resistance.

In the innermost layer, HfO_xC_y species and SiO_xC_y species were observed, the latter at the interface between $MoSi_2$ and HfC. The formation of SiO_xC_y species could to be related again to interaction of CO species with $MoSi_2$ at the very low oxygen partial pressure existing under the scale. The oxidation mechanisms of this composite still have to be completely understood and will be object of further investigation.

As for the diboride system, the role of atomic oxygen is unclear. In the literature no studies can be found on this topic. The microstructural features of the HfC-based material after testing in the arc-jet facility are indeed very similar to those of samples oxidised in conventional furnaces.

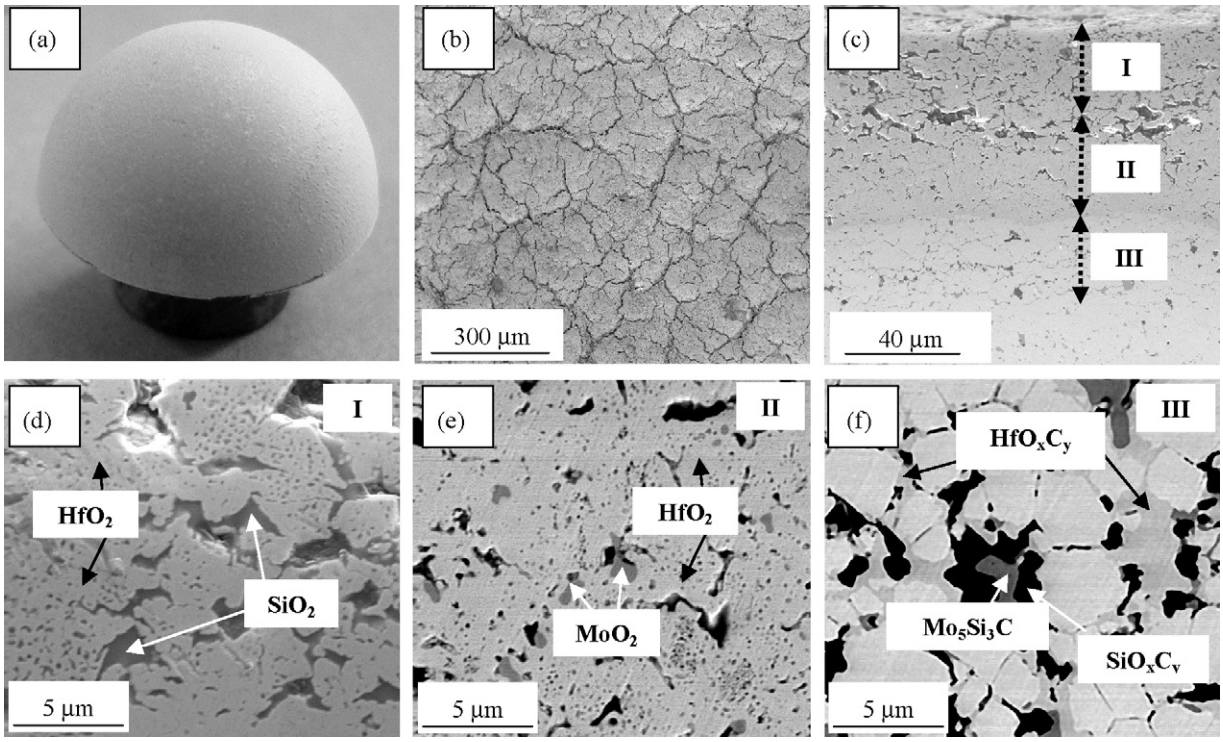

Fig. 7. (a) HfC sample after arc-jet test, (b) surface, (c) cross section. Enlarged view of (d) layer I (SE imaging), (e) layer II (BSE imaging), (f) layer III (BSE imaging).

4. Numerical rebuilding for surface catalytic efficiency evaluation

Numerical computations were carried out using the model described in Section 2.3, under different assumptions about the catalytic properties of the specimen surface with reference to catalytic efficiency of atomic nitrogen and oxygen. The simulations refer to the four plasma torch test conditions reported in Table 2. Based on the computed heat flux distributions, a thermal analysis was carried out to evaluate the catalytic efficiency value γ needed to fit the experimental temperature data. The catalytic efficiency is defined as the ratio of the number of dissociating atoms that recombine at the wall to the total number of the colliding atoms with the wall. For a non catalytic wall this value is 0, while for a fully catalytic wall this is 1. Fig. 8 shows the steady state results computed under the two assumptions of fully catalytic and non catalytic wall and the experimental data obtained with the pyrometer for both material samples. For thermal analysis, input values of specific heat and thermal conductivity are necessary. As a first approximation, the values of monolithic HfC and HfB_2 were considered for the composites, as follows: 200 J/(kg °C) and 22 W/m °C for specific heat and

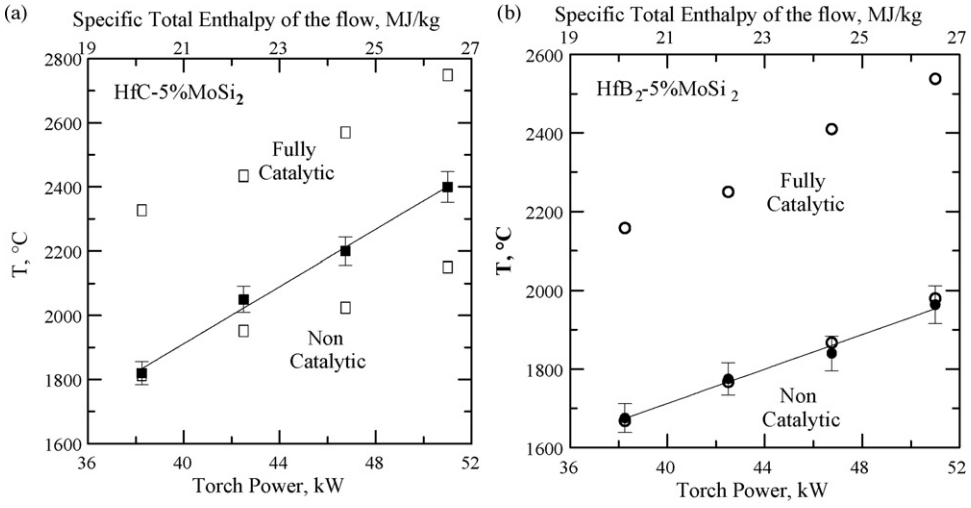

Fig. 8. Experimental results and numerical solutions corresponding to the different assumption of fully catalytic (FC) and non catalytic (NC)wall for (a) HfB2 and (b) HfC.

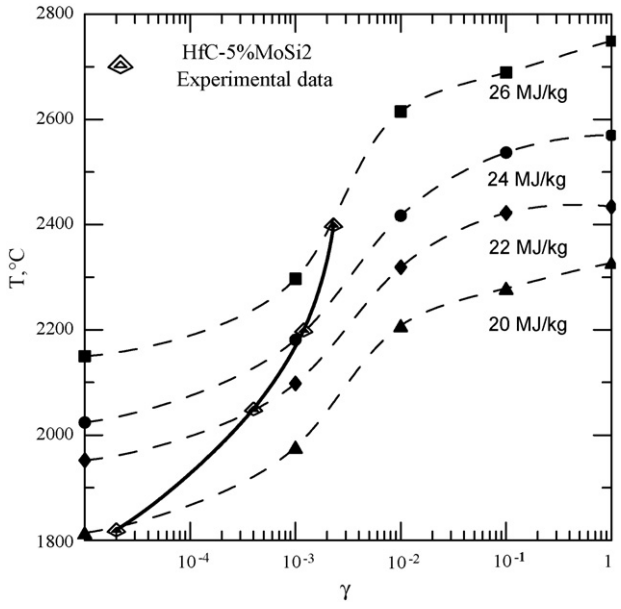

Fig. 9. Numerical evaluation of coefficient of catalytic recombination for HfC-5% $MoSi_2$ as a function of the temperature.

thermal conductivity of HfC,[27] 300 J/(kg °C) and 80 W/m °C for specific heat and thermal conductivity of HfB_2.[28] The data displayed in Fig. 8a and b, at the same plasma torch conditions, i.e. the same free stream conditions, highlight that the heating behaviour of the two materials was different. The experimental results of HfB_2 sample matched well the numerical values corresponding to the non catalytic wall condition. This points out that the material herein tested exhibits a non catalytic behaviour at very high temperatures. This behaviour can be explained by the formation of a silica surface layer (Fig. 6) which is known to possess very low catalytic recombination behaviour.[29,30] The presence of such a surface layer also justifies the high values of the surface emissivity, according to the literature data.

The experimental results for HfC suggested a partially catalytic behaviour. In order to identify a dependence of surface catalytic efficiency with temperature, different values were considered for each test conditions. Fig. 9 shows the results of the computations. At 1800 °C HfC exhibited a non catalytic behaviour. Increasing the temperature the catalytic efficiency increased up to a value of 2×10^{-3} at 2400 °C (Fig. 4a and b) which is relatively low with respect to the fully catalytic wall condition ($\gamma = 1$) and of the same order of other low catalytic materials such as those of the Space Shuttle tiles.[31]

It should be pointed out that the present tests have been carried out at atmospheric pressure conditions. Experimental and theoretical works on the catalytic activity of silica-based materials under simulated re-entry conditions[32,33] showed that at constant temperature the catalytic atomic recombination coefficients are decreasing functions of the pressure. Therefore the catalytic properties of the material, in respect to the recombination of oxygen atoms, may be larger at lower pressures, as found for instance in arc-jet experiments with ZrB_2/SiC and HfB_2/SiC ceramic materials.[2]

5. Summary and future work

Two different ultra-high temperature ceramics, HfB_2 + 5% $MoSi_2$ and HfC + 5% $MoSi_2$ were produced by pressureless sintering. Machined hemispherical models were exposed to ground simulated atmospheric re-entry conditions using arc-jet testing, with an average specific total enthalpy of the flow around the body of the order of 5–10 MJ/kg and at atmospheric pressure.

The HfB_2 + 5% $MoSi_2$ model surface reached a peak value of 1950 °C for H approaching 8 MJ/kg. SEM–EDS analysis of the cross section after exposure showed the formation of a compact silica oxide (about 15 μm) which sealed the underlying HfO_2 scale.

The HfC + 5% $MoSi_2$ model surface reached peak values of 2100 °C and 2400 °C. Cross section analysis showed a layered structure, constituted of an outer layer of porous HfO_2 and an inner layer mainly constituted of HfO_2 and silica.

Numerical calculations, which simulated the chemical non-equilibrium flow around the hemispheric model correlated well with the experimental results assuming a very low catalytic surface behaviour for HfB_2 and a catalytic behaviour increasing with temperature for HfC.

Although more testing is necessary to improve our understanding of the oxidation mechanisms under extreme conditions, the composites presently tested showed an excellent resistance to high enthalpy hot flows. This stability at temperature around 2000 °C opens up new developments in several fields of application, including nuclear applications and industries where extreme conditions are involved. Moreover, the possibility to produce near net shape components through a conventional sintering technique represents a technological advantage in comparison with materials in need of pressure-assisted techniques and expensive post-sintering machining.

References

1. Upadhya, K., Yang, J. M. and Hoffman, W., Materials for ultrahigh temperature structural applications. *Am. Ceram. Soc. Bull.*, 1997, **76**(12), 51–56.
2. Marschall, J., Chamberlain, A., Crunkleton, D. and Rogers, B., Catalytic atom recombination on ZrB_2/SiC and HfB_2/SiC ultrahigh-temperature 511 ceramic composites. *J. Spacecraft Rockets*, 2004, **41**(4), 576–581.
3. Gasch, M., Ellerby, D., Irby, E., Beckman, S., Gusman, M. and Johnson, S., Processing, properties and arc-jet oxidation of hafnium diboride/silicon carbide ultra high temperature ceramics. *J. Mater. Sci.*, 2004, **39**, 5925–5937.
4. Bongiorno, A., Forst, C. J., Kalia, R. K., Li, J., Marschall, J., Nakano, A. *et al.*, A perspective on modelling materials in extreme environments: oxidation of ultrahigh-temperature ceramics. *MRS Bull.*, 2006, **31**, 410–418.
5. Richet, N., Lespade, P., Goursat, P. and Laborde, E., Oxidation resistance of HfB_2–SiC coatings for protection of carbon fiber based composites. *Key Eng. Mater.*, 2004, **264–268**(TTP), 1047–1050.
6. Janowski, R., Tauche, M., Scheper, M., Monti, R. and Savino, R., Spaceplane: a new way for atmospheric reentry. In *Proceedings of the 1st Inter-national ARA Days, Atmospheric Reentry Systems, Missions and Vehicles. Session 15-System Design*, 2006.
7. Monti, R., De Stefano Fumo, M. and Savino, R., Thermal shielding of a reentry vehicle by ultra high temperature ceramic materials. *J. Thermophys. Heat Transfer*, 2006, **20**(3), 500–506.
8. Campbell, I. E. and Sherwood, E. M., ed., *High-Temperature Materials and Technology*. Wiley, New York, 1967.

9. Clougherty, E. V. and Kaufman, L., Investigation of boride compounds for very high temperature applications, ManLabs, Inc., Cambridge, MA, Air Force Technical Documentary Report No. RTD-TDR-63-4096, 1963.
10. Levine, S. R. *et al.*, Evaluation of ultra-high temperature ceramics for aero-propulsion use. *J. Eur. Ceram. Soc.*, 2002, **22**(14–15), 2757–2767.
11. Fahrenholtz, W. G. and Hilmas, G. E., NSF-AFOSR Joint Workshop on Future Ultra-High Temperature Materials, National Science Foundation Workshop, Arlington, VA, 13–14 January 2004. http://web.umr.edu/∼uhtm/.
12. Opeka, M., Talmy, I. G., Wuchina, E. J., Zaykoski, J. A. and Causey, S. J., Mechanical, thermal and oxidation properties of refractory hafnium and zirconium. *J. Eur. Ceram. Soc.*, 1999, **19**, 2405–2414.
13. Wuchina, E., Opeka, M., Causey, S., Spain, J., Cull, A., Routbort, J. *et al.*, Designing for utrahigh-temperature applications: the mechanical and thermal properties of HfB_2, HfC_x, HfN_x and αHf(N)). *J. Mat. Sci.*, 2004, **39**, 5939–5949.
14. Silvestroni, L. and Sciti, D., Effects of $MoSi_2$ additions on the properties of Hf– and Zr–B_2 composites produced by pressureless sintering. *Scripta Mater.*, 2007, **57**, 165–168.
15. Sciti, D. and Silvestroni, L., High-density pressureless sintered HfC-based composites. *J. Am. Ceram. Soc.*, 2006, **89**(8), 2668.
16. Jeng, Y. L. and Lavernia, E. J., Review, Processing of molybdenum disilicide. *J. Mat. Sci.*, 1994, **29**, 2557–2571.
17. Monteverde, F. and Savino, R., Stability of ultra-high-temperature ZrB_2–SiC ceramics under simulated atmospheric re-entry conditions. *J. Eur. Ceram. Soc.*, 2007.
18. Park, C., *Nonequilibrium Hypersonic Aerothermodynamics*. John Wiley &Sons, 1990.
19. Park, C., Review of chemical-kinetic problems of future NASA missions. I. Earth Entries. *J. Thermophys. Heat Transfer*, 1993, **7**(3), 385–398.
20. Park, C., Howe, J. T., Jaffe, R. L. and Chandler, G. V., Review of chemical-kinetic problems of future NASA missions. II. Mars entries. *J. Thermophys. Heat Transfer*, 1994, **8**(1), 9–23.
21. Park, C., Jaffe, R. L. and Partridge, H., Chemical-kinetic parameters of hyperbolic earth entry. *J. Thermophys. Heat Transfer*, 2001, **15**(1), 76–90.
22. Scatteia, L., Borrelli, R., Casentino, G., Beche, E., Sans, J. L. and Balat-Pichelin, M., Catalytic and radiative behaviours of ZrB_2–SiC ultra-high temperature ceramic composites. *J. Spacecrafts Rockets*, 2006, **43**, 1004–1012.
23. Berkowitz-Mattuck, J. B., High-temperature oxidation. III-Zirconium and hafnium diborides. *J. Electrochem. Soc.*, 1966, **113**, 908.
24. Wang, C. R. and Yan, J. M., Thermal stability of refractory carbide/boride composites. *Mat. Chem. Phys.*, 2002, **74**, 272–281.
25. Lohfeld, S. and Schütze, M., Oxidation behaviour of particle reinforced MoSi2 composites at temperatures up to 1700 °C. Part I: Literature review. *Mater. Corr.*, 2005, **56**(2), 93–97.
26. Bargernon, C. B., Bendon, R. C., Jette, A. N. and Phillips, T. E., Oxidation of Hafnium carbide in the temperature range 1400° to 2060 °C. *J. Am. Ceram. Soc.*, 1993, **76**, 1040–1046.
27. Loehman, R., Corral, E., Dumm, H. P., Kotula, P. and Tandon, R., Ultra High Temperature Ceramics for Hypersonic Vehicle Applications, SANDIA REPORT SAND 2006-2925, June 2006, Sandia National Laboratories, Albuquerque, New Mexico, USA.
28. Krajewski, A., D' Alessio, L. and De Maria, G., Physic-chemical and thermo-physical properties of cubic binary carbides. *Cryst. Res. Technol.*, 1998, **33**, 34.
29. Greaves, J. C. and Linnett, J. W., Recombination of atoms at surfaces. Part 5. Oxygen atoms at oxide surfaces. *Trans. Faraday Soc.*, 1959, **55**, 1346.
30. Dickens, P. G. and Sutcliffe, M. B., Recombination of oxygen atoms on oxide surfaces. Part 1. Activation energies of recombination. *Trans. Faraday Soc.*, 1964, **60**, 1272.
31. Gnoffo, P. A. and Inger, G. R., Analytic corrections to CFD heating predictions accounting for changes in surface catalysis, Part 2. *AIAA 7th International Spaceplanes and Hypersonic Systems and Technologies Conference*, Norfolk, VA, November 18–22, 1996, AIAA Paper No. 96-4589.
32. Kolesnikov, A. F., Gordeev, A. N., Vasilevskii, S. A. and Verant, J. L., Predicting catalytic properties of SiC material for the Pre-X vehicle reentry conditions. In *Proceedings of the First European Conference for Aerospace Sciences (EUCASS)*, 2005.
33. Kolesnikov, A. F., Yakushin, M. I., Pershin, I. S., Vasilevskii, S. A., Chaot, O., Vancrayenest, B. *et al.*, Comparative study of surface catalytic under subsonic air test conditions. In *Proceedings of the 4th Europ. Symp. Aerothermodynamics for Space Applications*, 2001, pp. 481–486, ESA SP-487.